Eigenchannel R-matrix calculation of the J=1 odd-parity spectrum of barium

To cite this article: M Aymar 1990 *J. Phys. B: At. Mol. Opt. Phys.* **23** 2697

J. Phys. B: At. Mol. Opt. Phys. 23 (1990) 2697–2716. Printed in the UK

Eigenchannel R-matrix calculation of the $J = 1$ odd-parity spectrum of barium

Mireille Aymar

Laboratoire Aimé Cotton, CNRS II, Bâtiment 505, 91405 Orsay Cedex, France

Received 18 April 1990

Abstract. The $J = 1$ odd-parity spectrum of barium is studied through a combination of the eigenchannel R-matrix and multichannel quantum defect (MQDT) methods. Short-range parameters used by MQDT to describe electronic channel interactions are determined by performing R-matrix calculations in LS coupling and the (LS/jj) frame transformation is used to include fine-structure effects. This approach has proven to be an efficient tool for describing lighter alkaline earths but its ability to handle Ba, where spin–orbit interaction is stronger, is analysed for the first time. The calculations reproduce well the perturbations of the principal Rydberg series $6snp\ ^{1,3}P_1$ by eight low-lying doubly excited levels as well as most of the features observed in the photoabsorption spectrum $6s^2\ ^1S_0$ $J = 1^\circ$ up to the $6p_{3/2}$ threshold. Although some discrepancies were found, the considerable overall success obtained by describing spin–orbit effects in Ba with the (LS/jj) frame transformation instead of including them explicitly in the short-range calculation is a great surprise.

1. Introduction

In the last few years, several theoretical investigations devoted to Ca (Greene and Kim 1987, Kim and Greene 1987, 1988) and Sr (Aymar *et al* 1987, Aymar 1987, Aymar and Lecomte 1989, Kompitsas *et al* 1990) have demonstrated that a very realistic description of these atoms can be attained by combining the eigenchannel R-matrix method developed by Greene (1985, 1988) with the multichannel quantum defect theory (MQDT) (Seaton 1983, Fano and Rau 1986). Impressive agreement between theory and experiment has been obtained not only for the perturbed Rydberg series and photoabsorption spectra but also for other observables such as electron branching ratios and angular distributions.

Briefly, the theoretical procedure consists in calculating variationally with the R-matrix method the short-range parameters used by MQDT to describe channel interactions. R-matrix calculations are performed in LS coupling and the geometric frame transformation (LS/jj) is employed to account for fine-structure effects.

In recent years, with the development of multistep and multiphoton laser spectroscopy, an increased number of experimental investigations have dealt with alkaline earth atoms. By far, the barium spectrum has been the most thoroughly studied and the MQDT has enjoyed a remarkable success in interpreting experimental data (Aymar 1984). However the theoretical analyses use empirical MQDT parameters adjusted to agree with a particular set of measurements. The complexity of Ba is such that empirical MQDT treatments come up against some difficulties associated with the

0953-4075/90/162697+20$03.50

energy dependence of the parameters and with the very large number of parameters required. As experimental probes of channel mixing become increasingly more detailed this makes it desirable to develop improved techniques to calculate the MQDT parameters. Ba shares with the lighter alkaline earths a very strong channel mixing but compared to the lighter atoms the Ba spectrum is complicated by larger spin–orbit effects. The introduction of fine-structure effects using a frame transformation was found adequate to describe numerous effects of spin–orbit interaction which show up in the photoabsorption spectrum of Sr (Aymar 1987) and in the various observables investigated in Ca (Lange *et al* 1989) and Sr (Aymar and Lecomte 1989) using laser excitation techniques. In this treatment, spin–orbit effects are completely neglected within the reaction volume, i.e. at short range, but accounted for in the asymptotic region. The validity of such an approximation is more questionable in Ba than in the lighter alkaline earths. One major goal of the present study is to analyse the applicability of this approach to Ba.

This paper deals with the $J = 1$ odd-parity spectrum of Ba below the $6p_{3/2}$ threshold. On the experimental side, this spectrum has been extensively studied over the last two decades either in one-photon excitation from the the ground state (Garton and Codling 1960, Garton and Tomkins 1969, Garton and Parkinson 1974, Hudson *et al* 1970, Brown and Ginter 1978, Griesmann *et al* 1990) or using laser spectroscopy (Armstrong *et al* 1978, Kachru *et al* 1985, Sandner *et al* 1986). The perturbations of principal Rydberg series by high-lying doubly excited states as well as most of the features observed in the photoabsorption spectrum out of the ground state are successfully described using the approach developed for describing lighter alkaline earths. This is an unexpected result, considering the fact that previous studies seemed to indicate that the spin–orbit terms must be included in the short-range calculation instead of by the simpler (LS/jj) frame transformation. In this context, three previous studies relevant to the $J = 1$ odd-parity spectrum should be mentioned. The first ones are the empirical MQDT analyses of the bound spectrum performed by Armstrong *et al* (1978) and by Post *et al* (1986) respectively, where the (LS/jj) frame transformation has not been able to account for all the channel mixings. The last one is the calculation of the photoabsorpion spectrum performed by Bartschat *et al* (1986) using the standard formulation of the R-matrix method (Burke and Robb 1975); in this calculation spin–orbit terms were included explicitly in the short-range calculation.

Section 2 describes the computational procedure. The results relevant to either the bound or autoionising energy range are presented and compared with previous experimental and theoretical data in sections 3 and 4 respectively. Concluding remarks are given in section 5.

2. Computational procedure

Calculations are done by combining the eigenchannel R-matrix and MQDT methods, the computational procedures being similar to those previously used in Ca (Greene and Kim 1987, Kim and Greene 1987, 1988) and in Sr (Aymar 1987, Aymar and Lecomte 1989, Kompitsas *et al* 1990). Detailed accounts can be found in these papers and only some particular points and useful formulae are outlined here.

2.1. Eigenchannel R-matrix calculation in LS coupling

As in earlier studies in lighter alkaline earths, R-matrix calculations are performed in LS coupling. The LS-coupled wavefunctions of the pair of electrons outside a frozen

core are calculated variationally within a finite reaction volume V, using a variational expression for the normal logarithmic derivative on the surface S of V. We use a reaction volume of radius r_0=19 au; test calculations performed with $r_0 = 21$ au show only minor differences in the various final results.

As in previous eigenchannel R-matrix calculations, a model potential is used to describe the interaction of each valence electron with the closed shell core Ba^{2+}. It is well known that the d and mainly f orbitals of Ba^+ depend sensitively on the accuracy of the model potential because the electric attraction and the centrifugal repulsion balance each other critically (Griffin *et al* 1969, Connerade 1978). This balance expresses itself in the occurrence of a barrier which separates two valleys in the effective potential seen by a f electron. Because of this great sensitivity, we use for Ba^+ a potential somewhat more sophisticated than in Sr^+. The potential consists of a screening term and a polarisation term, both terms being l dependent

$$U(r) = -\frac{1}{r}[2 + 54\exp(-\alpha_1^l r) + \alpha_2^l r \exp(-\alpha_3^l r)] - \frac{\alpha_d}{2r^4}\{1 - \exp[-(r/r_c^l)^6]\}. \qquad (1)$$

The dipole polarisability α_d is fixed to 11.4 and the empirical parameters α_i^l and r_c^l are adjusted to obtain optimum agreement with the known spectrum of Ba^+. The empirical model potential reproduces accurately the average spin–orbit energies of s, p, d, f and g levels of Ba^+. Good energies are obtained even for the f levels particularly sensitive to centrifugal barrier effects as reflected by the anomalous evolution of their quantum defects.

Using the potential $U(r)$, a set of one-electron orbitals is calculated within V; two kinds of orbitals are considered which either vanish at $r = r_0$ (closed type) or have a non-zero amplitude at $r = r_0$ (open type). The two-electron basis functions of the form $nln'l'$ are antisymmetrised products of these orbitals of definite S, L and parity. The quantum numbers n, l, l' define a specific channel converging to the Ba^+ nl threshold. The two-electron basis functions are chosen to describe two different groups of channels. A first set contains the open or weakly closed channels in which the outermost electron can escape from the reaction volume. These channels require a closed-type orbital to describe the core electron and open- and closed-type orbitals for the excited or continuum electron. The second set of channels corresponds to the strongly closed channels which contribute at short range but are exponentially small on the surface of the reaction volume; they are described by closed-type orbitals only. These channels account for the polarisation distortion of the one-electron functions induced by the presence of the second electron.

Using trial functions which are linear combinations of chosen two-electron functions with unknown superposition coefficients, the variational principle provides the R-matrix eigenstates Ψ_β characterised by constant normal logarithmic derivatives b_β across the surface S. The expansion coefficients c_k^β and eigenvalues b_β are solutions of a generalised eigensystem which must be solved for each energy E at which the R-matrix is desired. Greene and Kim (1988) have shown recently that a transformation of the system in a new representation speeds up considerably this part of the computation. The transformed system is solved in a small amount of time on an arbitrary energy mesh. Using basis sets very similar to that used in a previous work (Aymar and Lecomte 1989) on Sr, three independent calculations are done for the $^1P^o$, $^3P^o$ and $^3D^o$ symmetries.

Outside the reaction volume, the R-matrix eigenstates are matched to Coulomb expansions, yielding LS-coupled short-range reaction matrices as explicit functions of

the energy E. The dimension of each LS-coupled short-range reaction matrix equals the number of open or weakly closed channels included in the R-matrix treatment.

2.2. MQDT treatment

The effects of fine stucture are included using a (LS/jj) geometric frame transformation which allows the LS-coupled reaction matrices to be recoupled into a larger jj-coupled reaction matrix $K(E)$ referring to the jj-coupled dissociation channels; this energy-dependent matrix furnishes all the information to characterise final state channel mixing. Calculation of photoabsorption strengths requires in addition the calculation of dipole matrix elements connecting the R-matrix eigenstates determined for the $^1P^o$ symmetry to the ground state. The ground state wavefunction is obtained by diagonalising the Hamiltonian using a basis set of two-electron functions involving closed-type orbitals only. Dipole matrix elements are calculated in the length and velocity formulation. Once the dipole matrix elements and the jj-coupled reaction matrix $K(E)$ are known, asymptotic boundary conditions are imposed by MQDT techniques. The only point at which fine structure enters this calculation is this last stage where the experimental spin–orbit split thresholds are used in the MQDT calculations.

Using standard MQDT techniques adapted to the bound or autoionising energy range, physical observables are calculated with energy-dependent MQDT parameters deduced from the $K(E)$ matrix. Within the eigenchannel MQDT formalism (Fano and Rau 1986 and references therein), the parameters are the eigenvalues μ_α and the eigenvectors $U_{i\alpha}$ of the short-range reaction matrix K. The orthogonal matrix $U_{i\alpha}$ connects the jj-coupled dissociation channels i to the K-matrix eigenchannels α which are LS coupled but correspond to mixed channels. Introducing an intermediate basis $\bar{\alpha}$ of strictly LS coupled channels, the $U_{i\alpha}$ matrix can be factorised in the form

$$U_{i\alpha} = \sum_{\bar{\alpha}} R_{i\bar{\alpha}} V_{\bar{\alpha}\alpha} \tag{2}$$

where the $R_{i\bar{\alpha}}$ corresponds to the standard (jj/LS) angular transformation and the $V_{\bar{\alpha}\alpha}$ are given by the R-matrix calculations.

In the autoionising energy range, in addition to the complete treatment enabling the determination of both the positions and profiles of the resonances, a treatment restricted to calculating the positions of autoionising levels can be carried out. As explained by Fano and Rau (1986), Lecomte (1987) and Kompitsas *et al* (1990), the position of resonant states can be obtained by using a contracted reaction matrix κ restricted to the closed channels

$$\kappa_{cc} = K_{cc} - K_{co}(iI_{oo} + K_{oo})^{-1}K_{oc} \tag{3}$$

where c denotes the closed channels, o the open channels, I a unit matrix and K the complete short-range reaction matrix referring to closed and open channels. Using the real part K_{eff} of κ, MQDT techniques adapted to bound spectra can be employed to obtain the resonance positions and the admixture coefficients of channel into each level.

3. Bound spectrum

A schematic diagram of the $J = 1$ odd-parity spectrum of Ba below the the $6p_{3/2}$ threshold is given in figure 1. The bound spectrum consists of the $6snp$ ^1P and ^3P

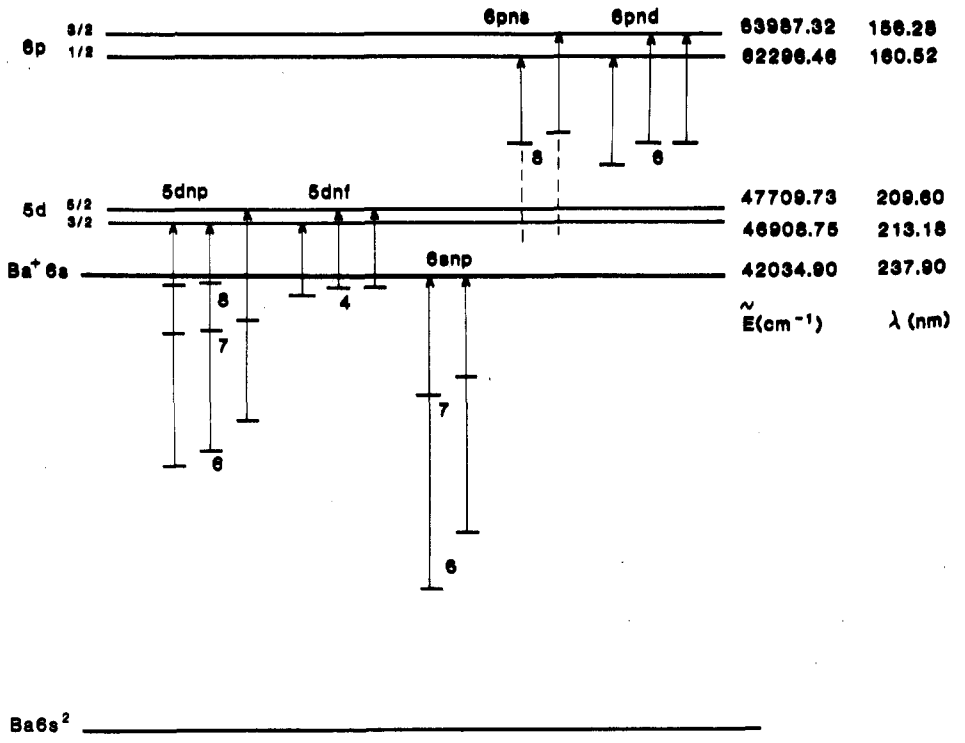

Figure 1. Schematic diagram of the $J = 1$ odd-parity spectrum of Ba below the $6p_{3/2}$ threshold. Energies $\tilde{E}$ (in cm^{-1}) and wavelengths λ (in nm) are referred to the Ba ground state.

series and of 12 doubly excited levels, lowest members of the 5dnp and 5dnf series converging to the $5d_{3/2,5/2}$ thresholds. Among the perturbers of the 6snp series is the 5d8p ^{1}P level, lying astride the ionisation limit, which strongly affects high-lying Rydberg levels. The perturbations of the principal series have been carefully analysed by Armstrong *et al* (1978) who used empirical MQDT parameters fitted to their experimental energy positions. Our aim is not to present a new analysis of the experimental energy data but rather to test the applicability of the R-matrix approach for describing such a complex spectrum, by far more complicated than the bound spectra of Ca and Sr which were successfully described using two-channel R-matrix calculations (Greene and Kim 1987, Aymar *et al* 1987). It is also of particular interest to see how the R-matrix treatment describes the oscillator strengths of the $6s^2\ ^1S_0$–$6sn$p $^1P_1$ transitions recently measured by Connerade *et al* (1988) up to $n = 42$.

We performed a eight-channel R-matrix calculation in which the channels converging to the 6s and 5d thresholds are treated as weakly closed whereas those having a 6p core are treated as strongly closed. This treatment is based on the surmise that the α channels are LS coupled, but apart from this assumption no approximation is made in determining the MQDT parameters, whose energy dependence is calculated explicitly. In contrast, Armstrong *et al* (1978) made several approximations in setting up their empirical eight-channel MQDT model. Their fit involves 15 parameters, more precisely eight eigenquantum defects μ_α and seven angles allowing the $V_{\bar{\alpha}\alpha}$ matrix of

equation (2) to be generated by successive rotations. In contrast with the R-matrix calculation, the α channels are not restricted to be LS coupled, angles coupling $\bar{\alpha}$ and α channels with different LS symmetries being found necessary to attain a good fit. Another approximation consists in neglecting the mixing between the 5dnp and 5dnf channels. A final difference with our treatment concerns the description of the energy dependence of the parameters : linear energy dependence is invoked for six parameters only. It is worth noting here that this previous analysis has reaveled the first case in which an energy dependent angle is required to fit bound levels.

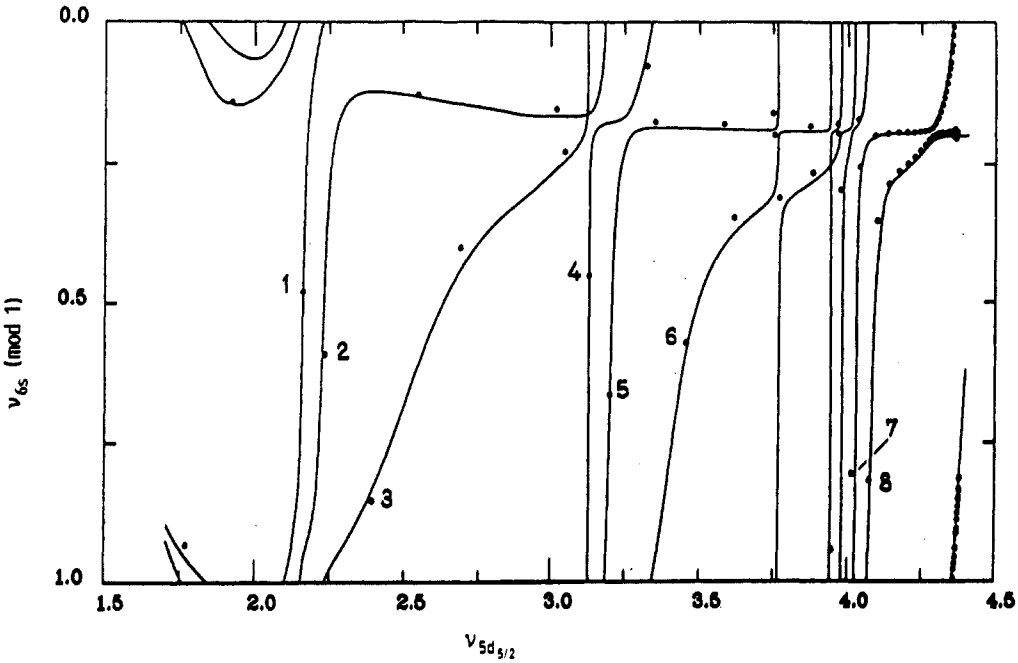

Figure 2. Lu–Fano plot of the $J = 1$ odd-parity bound levels in the $-\nu_{6s}$ (mod 1) against $\nu_{5d_{3/2}}$ plane. ——, present calculation; ●, experimental level positions: (1) 5d6p ^{3}D, (2) 5d6p ^{3}P, (3) 5d6p ^{1}P, (4) 5d7p ^{3}D, (5) 5d7p ^{3}P, (6) 5d7p ^{1}P, (7) 5d8p ^{3}D, (8) 5d8p ^{3}P (Moore 1952, Armstrong *et al* 1978, Post *et al* 1986).

Figure 2 gives a Lu–Fano plot of the eight interacting channels in the $-\nu_{6s}$ (mod 1) against $\nu_{5d_{5/2}}$ plane (ν_{6s} and $\nu_{5d_{5/2}}$ are the effective quantum numbers relative to the 6s and $5d_{5/2}$ thresholds respectively). The curve is the R-matrix result and the dots correspond to experimental data (Moore 1952, Armstrong *et al* 1978, Post *et al* 1986). This figure has to be compared with figure 11 of Armstrong *et al* (1978). On this latter figure, experimental points are exactly on the curve while some deviations are visible in figure 2. However, the agreement between R-matrix calculation and experiment is quite satisfactory accounting for the complexity of the spectrum. Clearly, the R-matrix approach correctly reproduces the pertubations of the 6snp series by the 5dnp levels labelled by the numbers (1) to (8). Note that no state deserves the label 5d8p ^{1}P, this level being spread out over a large number of high-lying 6snp levels; the perturbation of the high-lying Rydberg levels is perfectly reproduced by the calculation. The R-matrix calculation also correctly describes the weaker perturbations due to the 5d4f levels which occur for $3.75 < \nu_{5d_{5/2}} < 4$. Two improvements with respect to the

empirical study, must be noted. Firstly, the lowest levels 6s6p ^{1}P, ^{3}P and 5d6p ^{3}P, ^{3}D below $\nu_{5d_{5/2}} = 2.25$, disregarded by the empirical study, are accurately described by our calculation. The second improvement concerns the description of the 5dnf channels which are strongly closed in the low-energy range below $\nu_{5d_{5/2}} = 3.75$; in the empirical fit spurious 5d'3f' levels show up near $\nu_{5d_{5/2}} \sim 2.9$ whereas no 'vertical' branch occurs there in figure 2. These improvements are both due to the correct description of the energy dependence of the MQDT parameters which cannot be obtained empirically. In the present treatment, all the eigenquantum defects μ_α and matrix elements $V_{\bar{\alpha}\alpha}$ show a energy variation which, as illustrated later, departs strongly from a linear dependence.

The R-matrix μ_α values calculated at the threshold energy compare well with the empirical parameters while the $V_{\bar{\alpha}\alpha}$ matrix elements are rather different. The differences are related to the previously mentioned different approximations done in setting up the V matrix. We will return to this point later, but first an interesting comparison between the two treatments can be done which concerns the description of the interaction between the 6snp ^{1}P and 5dnp ^{1}P channels. By far, these channels are the most strongly mixed, as reflected by the marked curvature of the Lu–Fano curve near $\nu_{5d_{5/2}} = 2.5$, 3.5 and just below the 6s threshold. The eigenquantum defects and mixing angle derived for these two channels from the R-matrix calculation are compared with empirical parameters in figure 3. Good agreement is achieved in

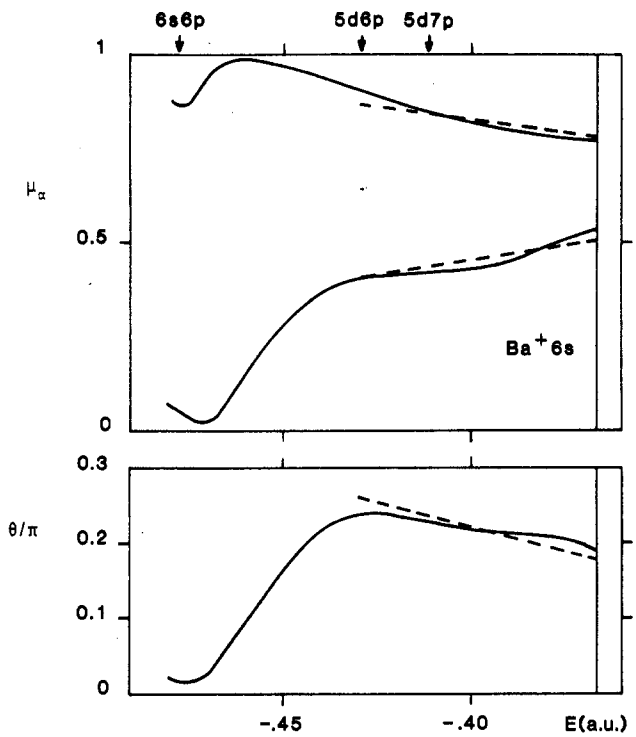

Figure 3. Eigenquantum defects μ_α and mixing angle θ for the 6snp ^{1}P and 5dnp ^{1}P channels as functions of the energy E (in au) referred to the double ionisation limit: ——, present calculation; – – –, Armstrong *et al* (1978). Some experimental levels are indicated by vertical arrows.

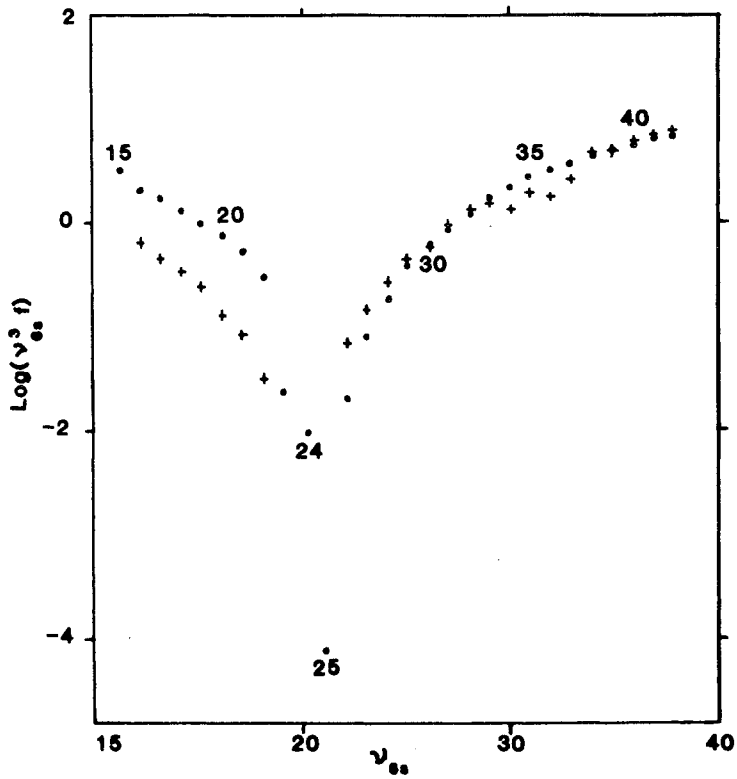

Figure 4. Oscillator strengths of the $6s^2\ ^1S_0$–$6snp\ ^1P_1$ transitions. The $\log(\nu^3_{6s}\ f)$ values are plotted as functions of ν_{6s}: ●, velocity results; +, Connerade *et al* (1990).

the high-energy range where the energy dependence of the parameters does not deviate much from a linear variation. The calculation clearly supports the energy dependence introduced for the θ angle in the empirical fit. The strong energy dependence below the energy position of the 5d6p ^{1}P level explains the inadequacy of the empirical MQDT model for describing the lower-lying levels. The mixing angle goes from zero at low energy to a maximum nearly equal to $\pi/4$ at higher energy where the two channels are essentially equally mixed. Very similar characteristics were found for the mixing angle between homologous channels of Ca (Greene and Kim 1987) and Sr (Aymar *et al* 1987) and also for the angle describing the $msnp$–$mpns$ interaction in Be ($m = 2$) and Mg ($m = 3$) analysed by O'Mahony and Greene (1985). This unusually large mixing, shared by all the alkaline earth atoms, is a signature of strong electronic correlations.

Turning back to the comparison of the calculated MQDT model with the empirical model of Armstrong *et al* (1978), it appears that two quite different sets of parameters give levels whose energies are close. However, as previously discussed (Aymar 1984), energy data are insufficient to test the validity of the assumptions made in setting up a MQDT model. Data on more sensitive observables are absolutely required to probe the wavefunctions. Post *et al* (1986) have analysed the hyperfine structure they observed in high-lying $6snp$ levels in terms of singlet–triplet mixing. The singlet–triplet mixing derived from the R-matrix calculation, very similar to that predicted by Armstrong

et al (1978) disagrees with these experimental results. Post *et al* (1986) have developed a five-channel MQDT model to reproduce both the data on energies and mixing coefficients. This treatment, restricted to high-lying levels, does not include the 5d*nf* channels. Large departures from the *LS* characterisation of the α channels are found necessary to reproduce the experimental singlet–triplet mixing. A detailed comparison of the the *R*-matrix MQDT parameters with the empirical parameters fitted by Post *et al* (1986) is not possible because the two treatments involve a different number of channels. However, many empirical $U_{i\alpha}$ parameters have non-zero values whereas the corresponding calculated matrix elements have zero values owing to the neglect of spin–orbit terms in the *R*-matrix calculations. Empirical MQDT parameters certainly do not represent only the short-range interactions but represent the aggregate influence of all forces that are not considered explicitly; thus it is not certain that the departures from the (LS/jj) frame transormation showed by the empirical MQDT studies are entirely related to the spin–orbit interaction. To clarify this point and analyse the origin of the discrepancy between experimental and calculated singlet–triplet mixing, additional theoretical works, such as *R*-matrix calculations including explicitly spin–orbit terms within the reaction volume, remain for future investigations.

We turn now to the oscillator strengths f of the $6s^2\ {}^1S_0$–$6snp\ {}^1P_1$ transitions. For high-lying levels, the known behaviour (Garton and Codling 1960, Parkinson *et al* 1976, Connerade *et al* 1988) deviates dramatically from a single ν_{6s}^{-3} law, with an intensity minimum near $n = 24$ and an enhancement of oscillator strengths at higher n. Figure 4 compares the *R*-matrix results with the recent experimental data obtained by Connerade *et al* (1988). The anomaly around $n = 24$ as well as the oscillator strengths of high-lying levels are perfectly reproduced whereas oscillator strengths are surestimated for the lower levels considered here; there, the predictions of the empirical study of Armstrong are in better agreement with experiment. The irregular behaviour of the f values is due to the 5d8p ^{1}P levels completely diluted in the high-lying Rydberg levels; the maximum of $(\nu_{6s}^3\ f)$ is found 3 cm^{-1} below the threshold, in agreement with the experiment which predicts the 5d8p ^{1}P to be located at the threshold.

4. Absorption spectrum

The absorption spectrum below the $6p_{3/2}$ threshold has been investigated by various experimentalists. Low-dispersion studies were performed by Garton and Tomkins (1969), Garton and Parkinson (1974) and Hudson *et al* (1970). Absolute values of photoionisation cross sections are reported by Hudson *et al* (1970) and Carlsten and McIlrath (1973). Brown and Ginter (1978) reinvestigated the 177–156 nm wavelength range with higher spectral resolution. Finally, new relative measurements were recently performed by Griesmann *et al* (1990) using synchrotron radiation. Comparison of our theoretical results with these experimental data as well as with the previous *R*-matrix calculation of Bartschat *et al* (1986) will be presented in two different regions. Section 4.1 concerns the range below the $5d_{3/2}$ threshold and section 4.2 the region between the $5d_{5/2}$ and $6p_{3/2}$ thresholds.

4.1. Absorption spectrum below the $5d_{3/2}$ threshold

In this region, we performed two different *R*-matrix treatments, namely a 13-channel calculation where all the channels converging to the 6s, 5d and 6p thresholds are

treated as open or weakly closed and an eight-channel treatment analogous to that performed below the 6s threshold. In this energy range, the 6p*n*d channels are actually strongly closed; treating them as weakly closed gives inaccuracies in the 13-channel MQDT calculation when introducing experimental energies for the threshold energies associated with these channels. To circumvent these difficulties related to the divergence of the Coulomb functions associated with these strongly closed channels, it was found necessary to use the same spin–orbit average theoretical energy for both $6p_{1/2}$ and $6p_{3/2}$ threshold energies. Under this condition, the 13-channel and eight-channel treatments give almost the same results over the entire energy range below the $5d_{3/2}$ threshold.

The absorption lines observed below the $5d_{3/2}$ threshold are due to 5d*n*p and 5d*n*f resonance members of six series converging to the $5d_{3/2}$ or $5d_{5/2}$ limits. Levels were previously classified using *Jl* (Garton and Tomkins 1969) or *LS* (Hudson *et al* 1970) designations. In fact no pure coupling scheme holds for most of the levels and here a *jj* designation is used.

Our eight-channel results are compared with experiments and previous theoretical predictions in figures 5–7, each figure corresponding to a different wavelength range. In each case, the upper curve A displays our velocity result; the vertical bars indicate the experimental resonance positions as observed by Garton and Tomkins (1969) or equivalently by Hudson *et al* (1970). Curves B and C correspond to the spectra observed by Hudson *et al* (1970) and Griesmann *et al* (1990) respectively. The lower broken curve, D, displays the theoretical results obtained by Bartschat *et al* (1986). Let us note that the absolute normalisation of the cross sections was not obtained by Griesmann *et al* (1990) and thus the vertical scale of curves B in figures 5–7 is chosen arbitrarily. Moreover the cross section scale used in curves B of figures 5–7 differs from those used in curves A and D of figures 5–7 by a factor of five. The assignments of each theoretical resonance (1) to (15) are displayed in table 1.

In the preceding section, it was shown that the *R*-matrix calculation perfectly reproduces the oscillator strengths of high-lying 6s*n*p ^{1}P levels affected by the 5d8p ^{1}P level. In figure 5 it can be seen that this level, corresponding to the large resonance (1) right on the 6s ionisation limit, dominates the near-threshold photoionisation. The large autoionisation width of this resonance spread on both sides of the 6s threshold reflects the above-mentioned strong mixing between the 6s*n*p ^{1}P and 5d*n*p ^{1}P channels. In this wavelength range, excellent agreement with experiment is achieved, a poorer description having been obtained using the conventional *R*-matrix method (Bartschat *et al* 1986). The comparison of curves A and C shows the absolute normalisation of the photoionisation cross sections observed by Hudson *et al* (1970) is too low by a factor of about five. This fact was already pointed out by Carlsten and McIlrath (1973); at 237.9 nm the revised value 50.8 ± 8 Mb proposed by these authors is in harmony with our velocity and length results 60.8 and 53.7 Mb respectively.

As can be seen from figure 6, in the wavelength range 233–237 nm, three resonant states have been observed, whereas our calculation gives five peaks labelled (3) to (7). In this range two levels, $5d_{5/2}5f[5/2]$ and $5d_{3/2}6f[5/2]$ respectively, are lacking in the table of Garton and Tomkins (1969). Clearly, our calculation overestimates the separation between both $5d_{5/2}5f$ levels (peaks (5) and (6)) which in fact merge into a unique resonance. The very small theoretical peak (7) is ascribed to the $5d_{3/2}6f[5/2]$ level which does not show up in the experimental spectra. Let us note that Bartschat *et al* (1986) also found a small peak at the same position. Another discrepancy between theory and experiment concerns the width of the resonance (3) which is underesti-

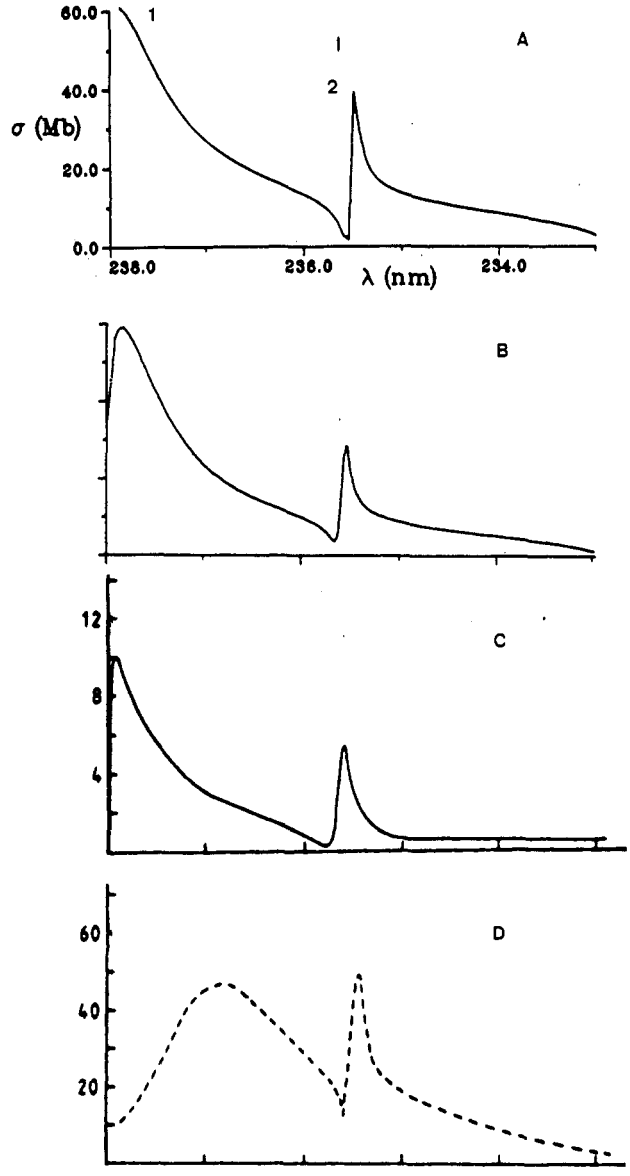

Figure 5. Total photoionisation cross section in the wavelength region from the 6s threshold to 233 nm. A, velocity results; vertical bars indicate experimental resonance positions as observed by Garton and Tomkins (1969) and Hudson *et al* (1970); the peak numbers refer to table 1. B, relative measurement of Griesmann *et al* (1990). C, absolute measurement of Hudson *et al* (1970). D, previous theoretical predictions of Bartschat *et al* (1986).

mated by our calculation.

Figure 7 illustrates the more complicated structure that emerges in the range 228–223 nm. We find eight resonant states in this region, the positions of which are in excellent agreement with experiments. Our calculation confirms the previous labels of

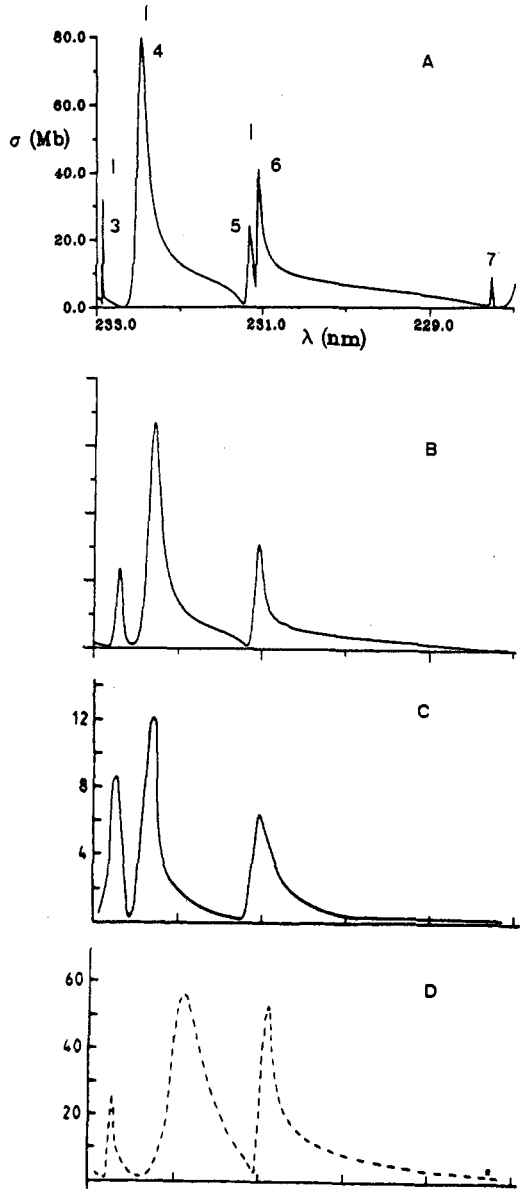

Figure 6. Same as figure 5 in the wavelength region from 233 to 228 nm.

configuration except for the peaks (11)–(13); however these three levels are so strongly mixed that our labels must be considered as tentative. Here also the calculated width of resonance (9), pertaining to the same series as resonance (3), is too small. In this wavelength range, comparison of the magnitude of computed and observed resonant peaks is meaningless, the energy mesh used in the MQDT calculation being smaller than the experimental resolution. In the wavelength range 233–222 nm, agreement between theory and experiment is comparable to that obtained by Bartschat *et al* (1986).

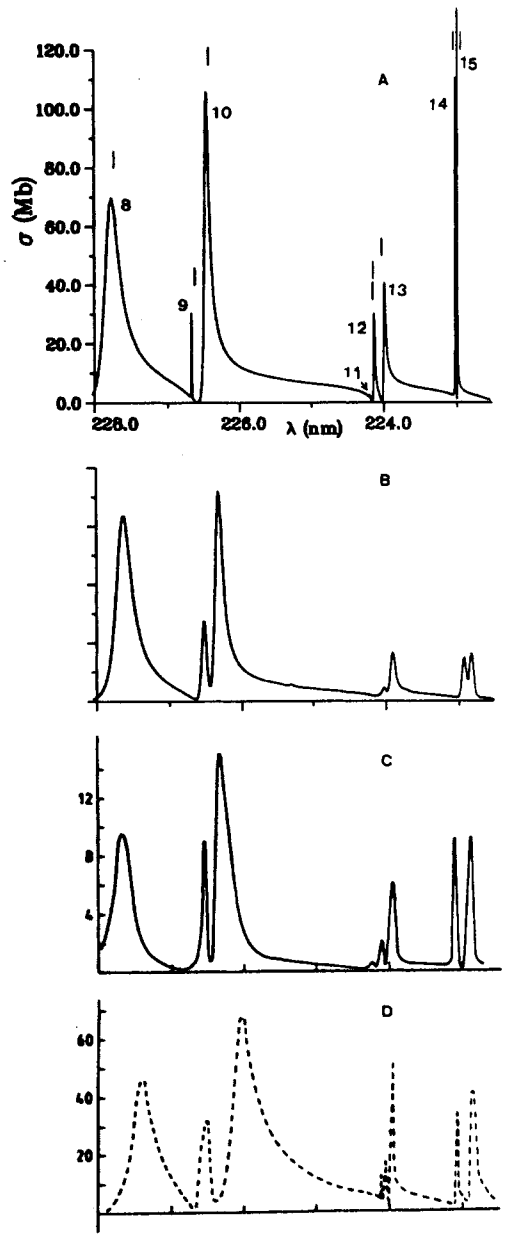

Figure 7. Same as figure 5 in the wavelength region from 228 to 222 nm.

A final comment concerns the 6p7s $^{1,3}P_1$ levels, lowest members of the 6p*n*s series, expected to lie within the spectral range below the $5d_{3/2}$ threshold. Our calculation confirms previous experimental studies, i.e. no particular structure can be ascribed to these levels, completely diluted into numerous resonances.

4.2. Absorption spectrum between the $5d_{5/2}$ and $6p_{3/2}$ thresholds

The structure of the absorption spectrum between the $5d_{5/2}$ and $6p_{3/2}$ thresholds is

Table 1. Level assignments of theoretical resonances in the wavelength range 228–223 nm.

Level	*jj* label[a]	*LS* label[b]	*Jl* label[c]
1	$5d_{5/2}8p_{3/2}$	$5d8p\ ^1P$	$5d_{5/2}8p[3/2]$
2	$5d_{3/2}5f_{5/2}$	$5d5f\ ^3P$	$5d_{3/2}5f[3/2]$
3	$5d_{3/2}9p_{3/2}$	$5d9p\ ^3D$	$5d_{3/2}9p[3/2]$
4	$5d_{3/2}9p_{1/2}$	$5d9p\ ^3P$	$5d_{3/2}9p[1/2]$
5	$5d_{5/2}5f_{7/2}$	$5d5f\ ^1P$	$5d_{5/2}5f[3/2]$
6	$5d_{5/2}5f_{5/2}$		
7	$5d_{3/2}6f_{5/2}$		
8	$5d_{5/2}9p_{3/2}$	$5d9p\ ^1P$	$5d_{5/2}9p[3/2]$
9	$5d_{3/2}10p_{3/2}$	$5d10p\ ^3D$	$5d_{3/2}10p[3/2]$
10	$5d_{3/2}10p_{1/2}$	$5d10p\ ^3P$	$5d_{3/2}10p[1/2]$
11	$5d_{5/2}6f_{5/2}$		$5d_{5/2}6f[1/2]$
12	$5d_{5/2}6f_{7/2}$	$5d6f\ ^1P$	$5d_{3/2}7f[3/2]$
13	$5d_{3/2}7f_{5/2}$	$5d7f\ ^3P$	$5d_{5/2}6f[3/2]$
14	$5d_{3/2}11p_{3/2}$	$5d11p\ ^3D$	$5d_{3/2}11p[3/2]$
15	$5d_{3/2}11p_{1/2}$	$5d11p\ ^3P$	$5d_{3/2}11p[1/2]$

[a] This work.
[b] Hudson *et al* (1970).
[c] Garton and Tomkins (1969).

due to transitions to the five 6p*n*s, *n*d channels. In this energy range we performed a 13-channel calculation, using now experimental values for all the threshold energies. This treatment enables the determination of both the positions and the profiles of the resonances. As documented later, the 6p*n*s, *n*d autoionising resonances are very broad and they overlap each other. As an attempt to identify all the resonances and to analyse the channel mixing, we carried out, in addition, a five-channel treatment based on the construction of an effective reaction matrix $K_{\rm eff}$ restricted to the 6p*n*s and 6p*n*d channels (see section 2.2). Results obtained in this latter analysis are presented firstly.

4.2.1. Positions of 6pns and 6pnd resonant levels. A Lu–Fano plot of the 6p*n*s, *n*d $J = 1$ levels on the $-\nu_{6p_{1/2}}$ (mod 1) against $\nu_{6p_{3/2}}$ (mod 1) plane is displayed in figure 8. The dots correspond to the experimental positions of the resonances observed by Brown and Ginter (1978) in the 60 000–62 200 cm^{-1} energy range ($5.246 < \nu_{6p_{3/2}} < 7.835$). The interactions between the various channels vary only slighty over this range and are described by the theoretical curve calculated for $6 < \nu_{6p_{3/2}} < 7$. Although some dots deviate from the curve, the overall agreement between theory and experiment is satisfactory, considering the fact that the underlying procedure is adequate to locate the position of each resonance with an error comparable to its autoionisation width. This figure has to be compared with figure 2 of Brown and Ginter (1978) which displays a hand-sketched Lu–Fano plot drawn through the same experimental data set. However, this latter curve was obtained using a four-channel MQDT model and thus differs from the present curve by the absence of the 'vertical' branch near $\nu_{6p_{3/2}}$ (mod 1) $\sim$ 0.25–0.35. It is evident from figure 8 that there is a strong mixing between the five 6p*nl* channels, the $6p_{1/2}ns$ and $6p_{1/2}nd_{3/2}$ series being strongly perturbed by the $6p_{3/2}nl$ levels. The $6p_{3/2}nd_{3/2}$, $6p_{3/2}nd_{5/2}$ and $6p_{3/2}ns_{1/2}$ are located near $\nu_{6p_{3/2}}$ (mod 1) $\sim$ 0.27, 0.40 and 0.75 respectively. The $6p_{3/2}nl$ character being spread over several energy levels, it is impossible to ascribe the $6p_{3/2}nl$

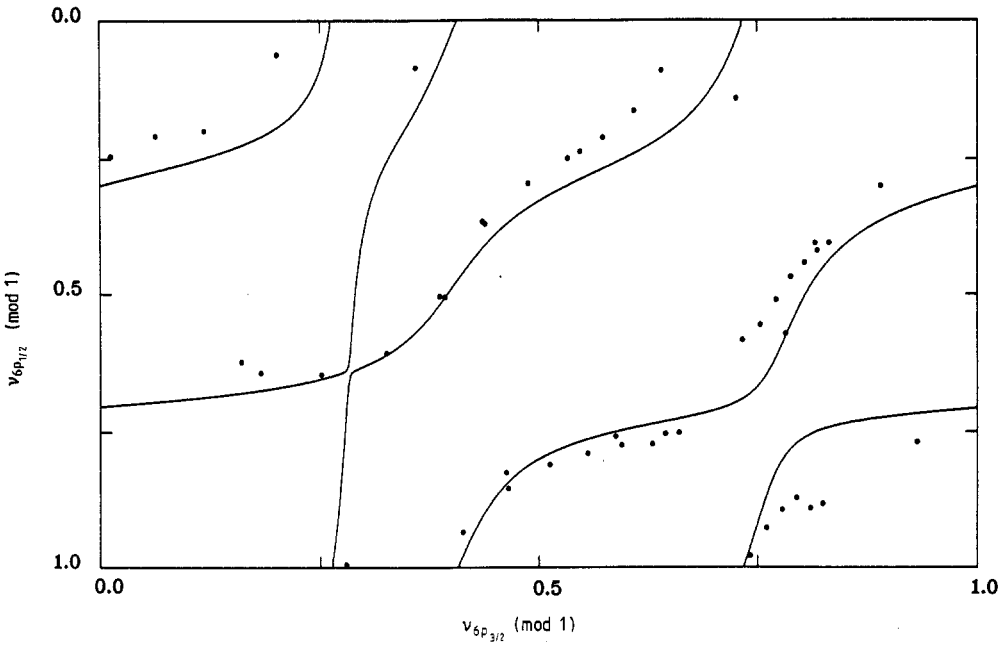

Figure 8. Lu–Fano plot $-\nu_{6p_{1/2}}$ (mod 1) against $\nu_{6p_{3/2}}$ (mod 1) below the $6p_{3/2}$ threshold: ——, present calculation; ●, experimental resonance positions (Brown and Ginter 1978).

perturbers to particular levels. Moreover the separations between the energy positions calculated with K_{eff} are often much smaller than the autoionisation widths and thus the number of theoretical energies is greater than the number of observed autoionising structures which actually correspond to several overlapping resonances. For all these reasons, assignment of a proper label to each observed resonance is meaningless. In particular, for most of the 6p*n*s, *n*d levels the classification proposed by Garton and Parkinson (1974) is not supported by our analysis. Although the present analysis does not permit us to label the observed resonances, it allows us to locate approximately the $6p_{3/2}nl$ levels and to better understand the underlying channel mixing.

4.2.2. Profiles of the 6pns and 6pnd autoionising resonances. Figure 9 compares our velocity result, curve A, below the $6p_{1/2}$ threshold with the recent measurement of Griesmann *et al* (1990), curve B, which is the sole measurement performed over the entire range from the $5d_{5/2}$ threshold to the $6p_{3/2}$ threshold. The agreement between theory and experiment is quite satisfactory, somewhat superior to that found below the $5d_{3/2}$ threshold.

More detailed results in the 210–170 nm wavelength range are displayed in figure 10. Our velocity and length results, curve A, are in good agreement stressing the convergence of the variational calculation. Moreover the present results better reproduce the experimental spectrum of Griesmann *et al* (1990), curve B, than the calculation performed by Bartschat *et al* (1986), curve C.

In the range around the $6p_{1/2,3/2}$ thresholds theoretical results are compared with the experimental spectra obtained by Brown and Ginter (1978) with a spectral resolution of 0.003 nm, about ten times better than that of Griesmann *et al* (1990). Results in the range from 60 000 cm^{-1} to the $6p_{1/2}$ threshold ($166.52 > \lambda > 160.52$) are shown in figures 11 and 12. Note the densitometer traces given without absolute

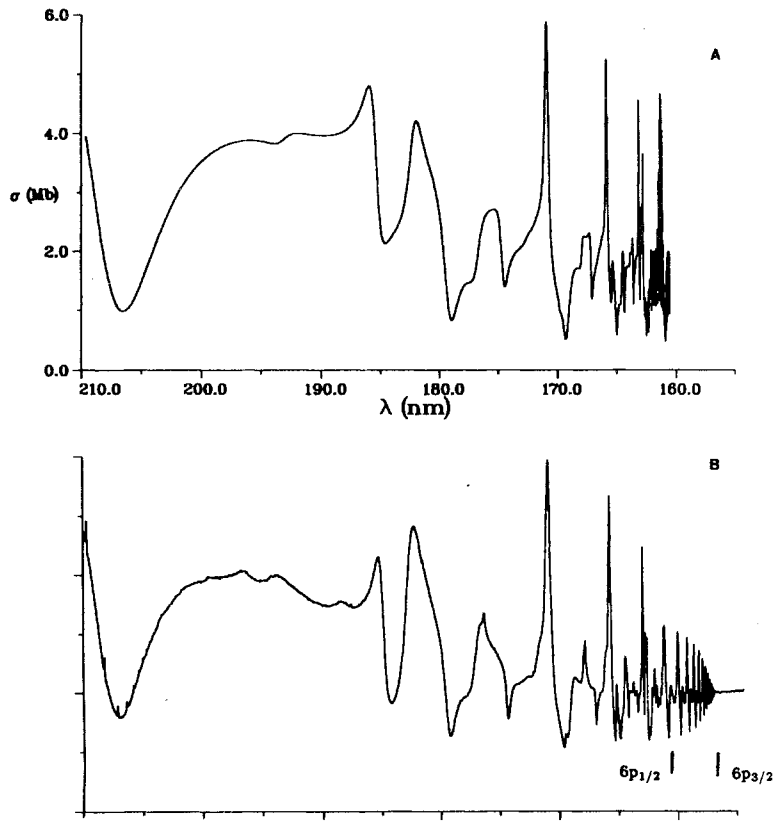

Figure 9. Total photoionisation cross section between the $5d_{5/2}$ and $6p_{3/2}$ thresholds. A, velocity results up to the $6p_{1/2}$ threshold. B, relative measurement of Griesmann *et al* (1990) up to the $6p_{3/2}$ threshold.

scale by Brown and Ginter (1978) have been converted into a photoionisation spectrum by inverting them and renormalising the overall magnitude to give optimum agreement with the calculated spectrum. Figure 11, curve A, illustrates the excellent agreement obtained between velocity and length results (for clarity only velocity results are shown in the higher energy range). Moreover, the calculation reproduces accurately the various characteristics of experimental resonances, curve B. As previously mentioned, the autoionisation structures are so broad and intermixed that we have not assigned labels to specific features. However the analysis of section 4.2.1 shows that the quasiperiodic enhancement of the cross sections is due to the presence of $6p_{3/2}nl$ levels strongly mixed with high-lying $6p_{1/2}ns$, nd Rydberg levels. The more pronounced enhancements near $\nu_{6p_{3/2}} \sim 5.4$, 6.4 and 7.4 are due to the $6p_{3/2}nd_{5/2}$ levels with $n = 8$, 9 and 10 respectively. The weaker enhancement visible just below the $6p_{1/2}$ threshold is due to the $6p_{3/2}$ 12s perturber.

Details of the range around 62 000 cm^{-1} are shown in figure 12. The $6p_{3/2}10d_{5/2}$ level can be discerned as a very broad resonance underlying the sharper lines of the $6p_{1/2}ns$, nd series. The positions and widths of calculated resonances, curve A, are in excellent agreement with experiment, curve B, while the description of the relative magnitude intensity of peaks is less satisfactory.

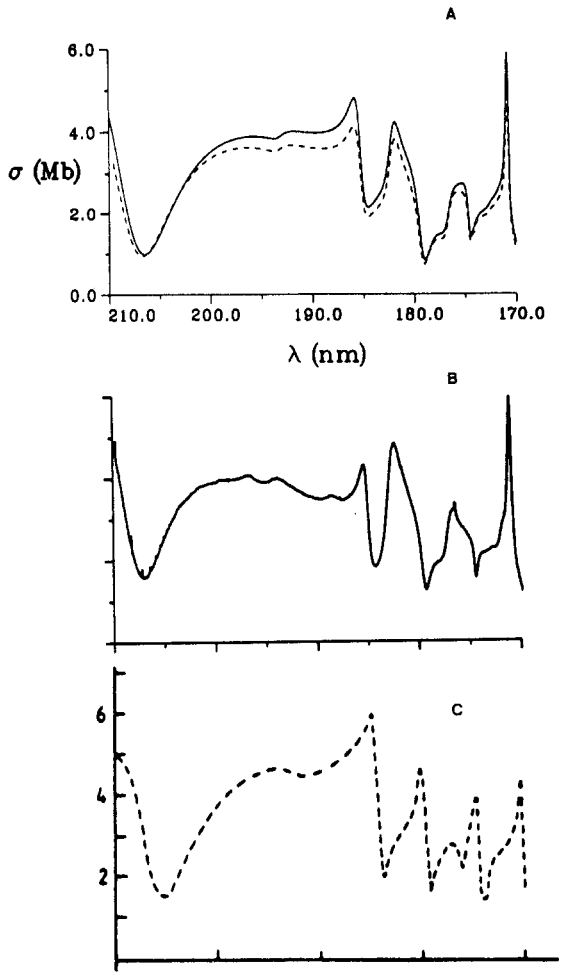

Figure 10. Total photoionisation cross section in the wavelength range from the $5d_{5/2}$ threshold to 170 nm. A, velocity (——) and length results (– – –). B, relative measurement of Griesmann *et al* (1990). C, previous theoretical predictions of Bartschat *et al* (1986).

The periodic intensity variation observed below the $6p_{1/2}$ threshold is still more evident above the threshold. Figure 13 shows that our calculation reproduces well the asymmetrical absorption/window profiles observed by Brown and Ginter (1978). It is worth noting here that similar asymmetrical absorption/window profiles have been observed also near the $4p_{1/2,3/2}$ thresholds of Ca (Brown and Ginter 1980) and near the $5p_{1/2,3/2}$ limits of Sr (Brown *et al* 1983) stressing again the great similarity between the heavy alkaline earths.

5. Conclusion

The present study has shown that the $J = 1$ odd-parity spectrum of Ba is generally well described by the approach combining the R-matrix and MQDT methods previously

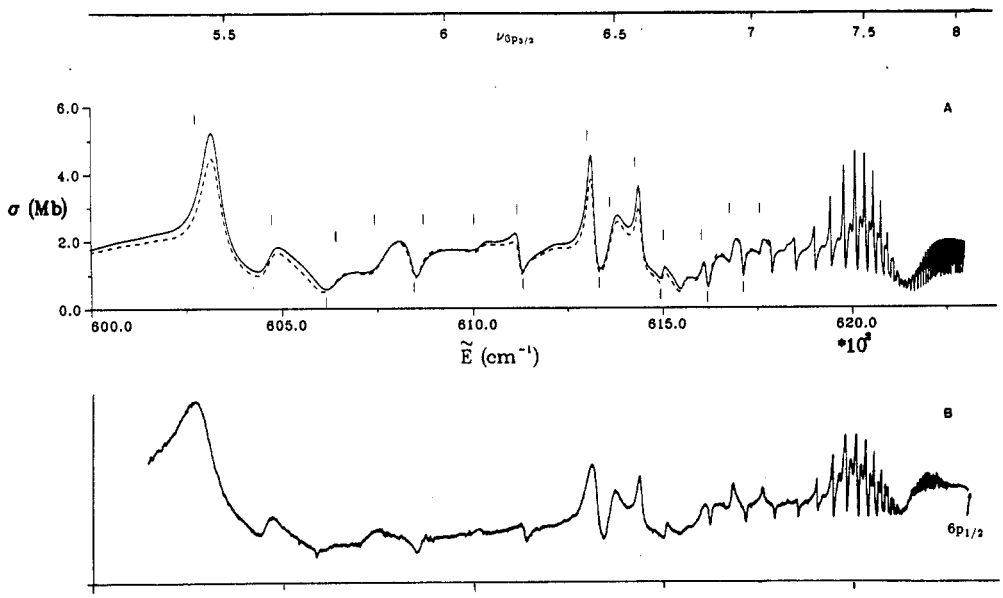

Figure 11. Total photoionisation cross section in the energy range from 60 000 cm^{-1} to the the $6p_{1/2}$ threshold. A, velocity (——) and length results (- - -). Vertical bars indicate the position of the observed absorption peaks and minima. B, relative measurement of Brown and Ginter (1978).

developed for handling lighter alkaline earths, the (LS/jj) frame transformation doing a surprisingly good job of describing spin–orbit effects. Without including explicitly the spin–orbit terms within the reaction volume as accomplished by Bartschat *et al* (1986), agreement between theory and experiment is better than that found by these authors or of the same quality.

The aim of the current line of research in alkaline earths through the joint use of MQDT and R-matrix methods is not only to obtain good agreement between theory and experiment but also to get a better understanding of correlation effects and to analyse systematic trends along the alkaline earths. Such information is difficult to extract from studies performed with the standard R-matrix method, whereas it is easily available once the jj-coupled short-range reaction matrix $K(E)$ is evaluated. Many similarities between Ba and the lighter alkaline earth atoms have been mentioned. All these atoms are dominated by an extremely strong electronic channel interaction. Because of this strong mixing, it is often meaningless to label the autoionising resonances observed in Ba with quantum numbers of independent particle states.

Some discrepancies were found between the calculated and measured absorption spectra and moreover the singlet–triplet mixing in high-lying $6snp$ levels is not correctly reproduced. To unravel the origin of these discrepancies and attempt to eliminate them, eigenchannel R-matrix calculations including the spin–orbit terms explicitly within the reaction volume have been undertaken. Preliminary calculations of the photoabsorption spectrum show very little differences with the present results (Greene and Aymar 1990).

To probe the reliability of the present calculations more thoroughly, it is of particular interest to extend the comparison between theory and experiment to observables

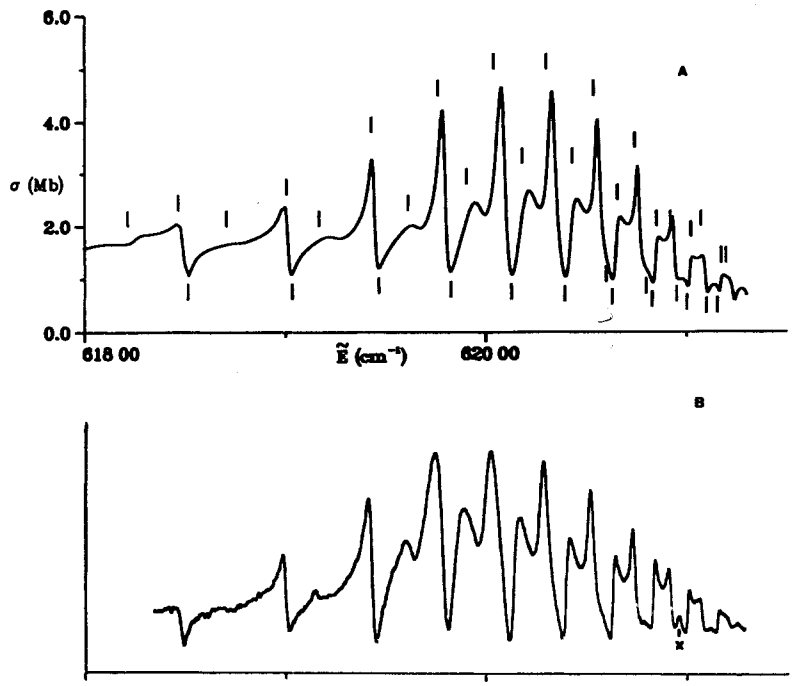

Figure 12. Same as figure 11 in the energy range from 61 800 to 62 130 cm^{-1} (the x in B denotes an impurity line).

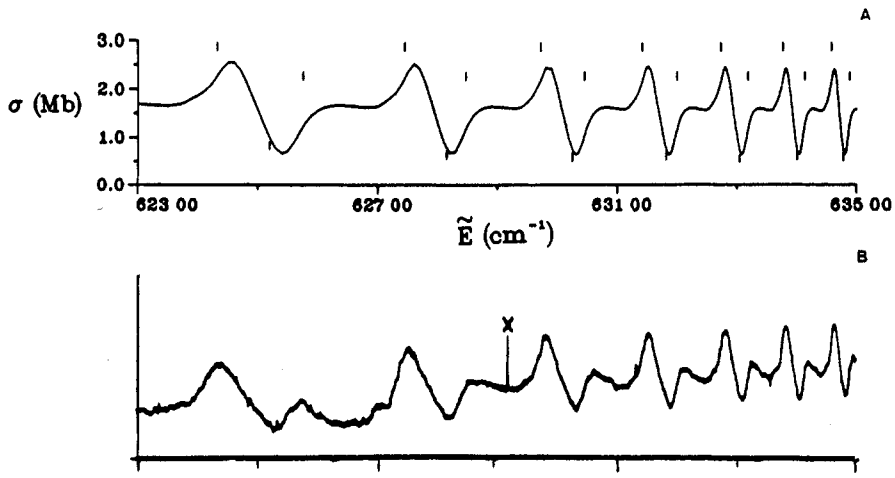

Figure 13. Same as figure 11 in the energy range from the the $6p_{1/2}$ threshold to 63 500 cm^{-1} (the x in B denotes an impurity line).

more sensitive to electronic channel and spin–orbit interactions than total photoionisation cross sections. This is possible in the $J = 1$ odd-parity spectrum of Ba, since the 6p*ns* $J = 1$ autoionising levels have been investigated using multistep laser excitation

(Kachru *et al* 1985, Sandner *et al* 1986). Recently a complete set of measurements has been achieved which includes absorption spectra, electron branching ratios and photoelectron angular distributions; preliminary results show a overall good agreement between these experimental data and the predictions obtained with the 13-channel reaction matrix K obtained in this work (Lange *et al* 1990).

Acknowledgments

I wish to thank C H Greene for valuable discussions and M L Ginter for sending me figures. I am indebted to U Griesmann for providing me with cross section photoionisation data prior to publication.

References

Armstrong J A, Wynne J J and Esherick P 1978 *J. Opt. Soc. Am.* **69** 211
Aymar M 1984 *Phys. Rep.* **110** 163
—— 1987 *J. Phys. B: At. Mol. Phys.* **20** 6507
Aymar M and Lecomte J M 1989 *J. Phys. B: At. Mol. Opt. Phys.* **22** 223
Aymar M, Luc-Koenig E and Watanabe 1987 *J. Phys. B: At. Mol. Phys.* **20** 4325
Bartschat K, Rudge M R H and Scott P 1986 *J. Phys. B: At. Mol. Phys.* **19** 2469
Brown C M and Ginter M L 1978 *J. Opt. Soc. Am.* **68** 817
—— 1980 *J. Opt. Soc. Am.* **70** 87
Brown C M, Longmire M S and Ginter M L 1983 *J. Opt. Soc. Am.* **73** 985
Burke P G and Robb D 1975 *Adv. At. Mol. Phys.* **11** 143
Carlsten J L and McIlrath T L 1973 *J. Phys. B: At. Mol. Phys.* **6** L284
Connerade J P 1978 *Contemp. Phys.* **19** 415
Connerade J P, Ma H, Shen N and Stavrakas T A 1988 *J. Phys. B: At. Mol. Opt. Phys.* **21** L241
Fano U and Rau A R P 1986 *Atomic Collisions and Spectra* (Orlando, FL: Academic)
Garton W R S and Codling K 1960 *Proc. Phys. Soc.* **75** 87
Garton W R S and Parkinson F R S 1974 *Proc. R. Soc.* A **341** 45
Garton W R S and Tomkins F S 1969 *Astrophys. J.* **158** 1219
Greene C H 1985 *Phys. Rev.* A **32** 1880
—— 1988 *Fundamental Process of Atomic Dynamics* ed J Briggs, H Kleinpoppen and H Lutz (New York: Plenum)
Greene C H and Aymar M 1990 to be published
Greene C H and Kim L 1987 *Phys. Rev.* A **36** 2706
—— 1988 *Phys. Rev.* A **38** 5953
Griesmann U, Esser B and Hormes J 1990 to be published
Griffin D C, Andrew K L and Cowan R D 1969 *Phys. Rev.* **177** 62
Hudson R D, Carter V L and Young P A 1970 *Phys. Rev.* A **2** 643
Kachru R, Tran N H, Pillet P and Gallagher T F 1985 *Phys. Rev.* A **31** 218
Kim L and Greene C H 1987 *Phys. Rev.* A **36** 4272
—— 1988 *Phys. Rev.* A **38** 2361
Kompitsas M, Cohen S, Nicolaides C A, Robaux O, Aymar M and Camus P 1990 *J. Phys. B: At. Mol. Opt. Phys.* **23** 2247–67
Lange V, Aymar M, Eichmann U and Sandner W 1990 to be published
Lange V, Eichmann U and Sandner W 1989 *J. Phys. B: At. Mol. Opt. Phys.* **22** L245
Lecomte J M 1987 *J. Phys. B: At. Mol. Phys.* **20** 3645
Moore C E 1952 *Atomic Energy Levels* NBS Circular No **467** vol II (Washington DC: US Govt Printing Office)
O'Mahony P F and Greene C H 1985 *Phys. Rev.* A **31** 250
Parkinson W H, Reeves E M and Tomkins F S 1976 *J. Phys. B: At. Mol. Phys.* **9** 157
Post B H, Vassen W and Hogervorst W 1986 *J. Phys. B: At. Mol. Phys.* **19** 511
Sandner W, Eichmann U, Lange V and Völkel M 1986 *J. Phys. B: At. Mol. Phys.* **19** 51
Seaton M J 1983 *Rep. Prog. Phys.* **46** 167